Astron. Astrophys. 357, 669–676 (2000)

ASTRONOMY AND ASTROPHYSICS

Improved isotopic ratio determinations in IRC+10216, the progenitor mass and the s process

C. Kahane[1], **E. Dufour**[1], **M. Busso**[2], **R. Gallino**[3], **M. Lugaro**[4], **M. Forestini**[1], **and O. Straniero**[5]

[1] Laboratoire d'Astrophysique de l'Observatoire de Grenoble B.P. 53, 38041 Grenoble Cedex 9, France
[2] Osservatorio Astronomico di Torino, 10025 Torino, Italy
[3] Dipartimento di Fisica Generale, Universitá di Torino, Via P. Giuria 1, 10125 Torino, Italy
[4] Department of Mathematics, Monash University, Clayton 3168, Victoria, Australia
[5] Osservatorio Astronomico di Collurania, 64100 Teramo, Italy

Received 17 December 1999 / Accepted 2 March 2000

Abstract. We present an improved determination of the chlorine isotopic ratio in the circumstellar envelope IRC+10216. This determination is the first clear evidence that in this circumstellar envelope elements heavier than the CNO do show deviations from the solar isotopic ratios, thus allowing a detailed comparison with quantitative model predictions. We have compared these data, together with other measurements for Mg and CNO isotopes, with predictions of AGB stellar models of solar metallicity and initial masses 1.5, 3 and 5 $M_\odot$ computed with the FRANEC evolutionary code. The comparison shows excellent agreement for the results of a low mass AGB model and remarkable disagreement for those of the 5 $M_\odot$ star. We briefly discuss the impact that model uncertainties can have on our conclusions.

Key words: nuclear reactions, nucleosynthesis, abundances – stars: AGB and post-AGB – stars: individual: IRC+10216 – stars: circumstellar matter – radio lines: stars

1. Introduction

In advanced asymptotic giant branch (AGB) evolutionary stages, H and He burning occur in two shells. The He-rich zone between them (hereafter defined as the He intershell) is periodically swept by convective instabilities induced by He-burning runaways (thermal pulses, TP), where ^{12}C is synthesized by partial He burning. In these layers heavy elements are built up by slow neutron captures (s process) on seed nuclei, driven by the ^{13}C(α,n)^{16}O and the ^{22}Ne(α,n)^{25}Mg reactions, as will be discussed in Sect. 4. After a few TPs, at the quenching of a thermal instability the H shell is inactive and the convective envelope penetrates in the upper region of the He intershell, bringing to the surface newly synthesized ^{12}C and s-processed elements. This recurrent phenomenon is known as *third dredge up* (TDU) (e.g., Busso et al. 1999).

Send offprint requests to: C. Kahane
(claudine.kahane@obs.ujf-grenoble.fr)

In AGB stars of mass lower than $M \simeq 3\,M_\odot$, the maximum temperature at the bottom of the convective instability barely reaches $T = 3\times10^8$ K in advanced TPs. At this temperature the ^{22}Ne neutron source is marginally activated. On average, about 1% of ^{22}Ne nuclei are burned, and rather small neutron fluxes are generated. The bulk of the neutron flux for the production of the heavy elements comes instead from the ^{13}C neutron source, which is activated at $T \leq 1\times10^8$ K and consumes all ^{13}C nuclei in radiative conditions during the interpulse period (Straniero et al. 1997). In contrast, in intermediate mass AGB stars ($M = 5$ to 8 $M_\odot$), the bottom temperature in the convective TPs reaches a peak value of 3.5×10^8 K and the ^{22}Ne(α,n)^{25}Mg reaction is efficiently activated (Iben 1975). Here, on average 30% of ^{22}Ne nuclei are consumed in the He intershell. On the other hand, in intermediate mass AGBs the mass of the He intershell is an order of magnitude lower than in AGB stars of lower mass, and the duration of the post-flash dip is shorter. Thus the ^{13}C pocket is expected to be comparatively less efficient (Vaglio et al. 1998; Straniero et al. 2000).

The s-process isotopes synthesized by the two neutron bursts described above belong to heavy elements from Sr to Pb (e.g., Truran & Iben 1977; Iben & Truran 1978; Gallino et al. 1998). Observationally, evidence of this dates back to the measurement of Tc in S stars (Merrill 1952). At the s-process efficiencies typical of S and C (type N) stars in the galactic disc the s-elements at the Zr or Ba abundance peaks are enhanced by up to one or two orders of magnitude (Busso et al. 1995). Unfortunately, this cannot be verified here, as no spectrocopic analysis is possible for the photosphere of CW Leo, the central object of the very dusty source IRC+10216.

In contrast, all nuclei lighter than Fe, though capable of capturing up to 50% of the available neutrons and hence to act as filters, or *poisons* for the neutron captures, reach only small enhancements, below $10-50$ in the He intershell and below $2-3$ in the envelope (Lugaro et al. 1999). This is so because of their high initial abundance and small neutron capture cross sections (the heavy isotopes beyond $A = 90$ have cross sections that are larger by up to three orders of magnitude). Despite this fact, intermediate mass nuclei from Ne to Fe can be used as indicators

Table 1. Telescope and spectra characteristics for the observed lines.

Line	Frequency (MHz)	η	HPBW (arcsec)	δv (km s^{-1})	T_{mb}^c (K)	$\int T_{mb}\mathrm{d}v$ (K km s^{-1})	v_{exp} (km s^{-1})
Na^{35}Cl (7-6)	91169.796 (0.065)	0.80	26	1.03	0.048 (0.013)	0.399 (0.024)	13.763 (0.220)
Na^{37}Cl (7-6)	89219.640 (0.122)	0.81	27	1.05	0.018 (0.007)	0.164 (0.022)	13.208 (0.428)
Al^{35}Cl(15-14)	218560.583 (0.068)	0.48	11	0.43	0.226 (0.029)	4.670 (0.193)	13.709 (0.094)
Al^{37}Cl(15-14)	213428.448 (0.064)	0.49	11	0.44	0.104 (0.027)	2.010 (0.068)	14.046 (0.089)

of the s-process conditions. Indeed, their final concentration is sensitive to the activation of the ^{22}Ne neutron source, hence to the maximum temperature achieved in the convective TPs. The Cl isotopic ratio shares this property. In particular, the neutron magic ^{37}Cl is relatively enhanced by the s process while the lighter ^{35}Cl, whose neutron capture cross section is a factor of 5 larger than that of ^{37}Cl, is depleted. Also the Mg isotope ratios are of interest. Both ^{25}Mg and ^{26}Mg are enhanced in the He intershell as a combination of α-captures on ^{22}Ne and of neutron captures, while ^{24}Mg remains almost untouched.

Thanks to the properties outlined above, the measurement of relative isotopic abundances of intermediate mass elements in the circumstellar envelopes of enshrouded AGB stars appears a powerful tool for studying the details of the s processing during thermal pulses, in particularly constraining the progenitor stellar mass.

Except for the lightest elements, isotopic shifts of the atomic lines are smaller than the thermal linewidths so that isotopic abundances are mainly derived from molecular lines, for which isotope shifts are easily resolved. The molecular rotational transitions of circumstellar molecules, observed in the radio millimeter range, have proved to be extremely useful for such determinations. In particular, towards the high mass-loss stars belonging to the end of the AGB phase, the optically thick dusty envelopes prevent any optical observation of the photospheric molecules, but the circumstellar molecules provide intense radio emission. Up to now, systematic measurements of the silicon, sulfur and chlorine isotopic ratios have been performed in a single circumstellar envelope, the carbon-rich IRC+10216. The central star, CW Leo, is a long period Mira-type variable, near the end of its AGB stage (Skinner et al. 1998) with a high mass loss rate of $\sim 1.5 \times 10^{-5}$ M$_\odot$ yr^{-1}. The luminosity is rather low, between 1.1 and 1.9 $\times 10^4$ L$_\odot$ (Groenewegen et al. 1998; Weigelt et al. 1998), depending on the precise value adopted for the distance, which is estimated to be in the range 130 to 170 pc (Le Bertre 1997; Winters et al. 1994). From models of the circumstellar emission, a C/O ratio ~ 1.4 and a total mass below 2 M$_\odot$ were estimated (Winters et al. 1994). However, if we accept for the distance a value close to the maximum allowed limit (170 pc), the derived luminosity might imply a more massive star, up to $4 - 4.5$ M$_\odot$ (Weigelt et al. 1998). This higher mass estimate was found by Guélin et al. 1995 to be compatible with some of the observed isotopic ratios. On the basis of new measurements for Cl isotopes and of a reanalysis of published data for other species, we plan to readdress here the problem of the progenitor mass of IRC+10216.

The chlorine isotopic ratio derived from the previous 2mm survey showed a quite large uncertainty. Additional observations have been performed and are presented in Sect. 2. The chlorine isotopic ratio, based on a careful compilation of all existing measurements, is derived with better accuracy and analyzed in Sect. 3, together with those of other intermediate atomic mass elements. Sects. 4 and 5 present an analysis of the envelope isotopic composition of intermediate mass elements, as expected from AGB nucleosynthesis models, to be compared with the observed ratios. Finally, Sect. 6 summarizes the main results of this research.

2. Observations and data reduction

The NaCl and AlCl data presented here were obtained with the 30m IRAM telescope in Pico Veleta, Spain between Nov. 29, 1997 and Dec. 1, 1997. The telescope was equipped with three SIS receivers (two in the 3mm range and one in the 1mm range) operating simultaneously, tuned in single side band (SSB) mode. The image sideband rejection was measured to be high (from 20 dB to 30 dB). The antenna temperature scale was calibrated every 10 minutes by the cold load technique. The main beam temperatures, T_{mb}, reported here are related to the antenna temperature scale, T_A^*, by $T_{mb} = T_A^*/\eta$ where η is the ratio of the main beam to the forward efficiency, as listed in Table 1. The absolute calibration accuracy was estimated to be of the order of 10%, from comparison with standard calibration spectra and from day to day line intensity variations. The antenna pointing was checked approximately every hour using the 115 GHz continuum receiver on a nearby bright quasar taken from the standard IRAM catalog. The typical pointing drift during one hour was 3″, significantly smaller than the telescope beam sizes (HPBW) given in Table 1. The signal from each receiver was sent to a filter bank with 256 channels of 1 MHz and to an autocorrelator with a resolution of about 80 kHz for the 3mm range lines and about 300 kHz for the 1mm range lines. The weather conditions were good, with typical SSB system noise temperatures between 250 and 300 K in the 3mm range and between 550 and 700 K in the 1mm range.

The observed NaCl and AlCl spectra are shown in Fig. 1 and Fig. 2. The NaCl spectra have been smoothed to a velocity resolution (δv) of about 1 km s^{-1} to increase the signal to noise ratio, whereas the AlCl spectra show their original resolution of about 0.44 km s^{-1}. Only linear or parabolic baselines have been subtracted from the spectra.

In order to derive the line characteristics, the observed profiles have been fitted to model profiles, which are, as usual for

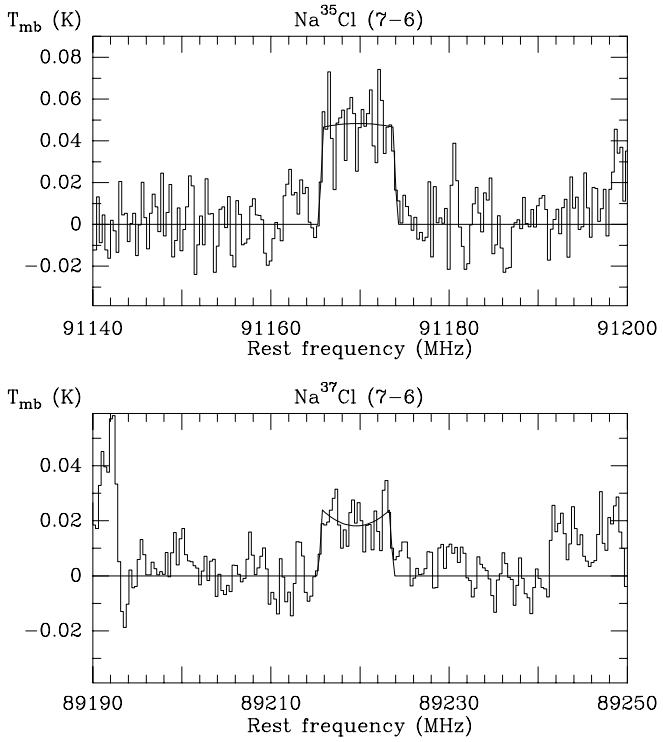

Fig. 1. NaCl (7-6) isotopomers lines observed towards IRC+10216 with the IRAM 30m telescope. The source position is α(1950) =09h45m14.8s and δ(1950) = 13°30′40″. The spectral resolutions are 1.03 and 1.05 km s^{-1}, respectively. Only linear or parabolic baselines have been subtracted and the solid lines represent the model profiles fitted to the lines.

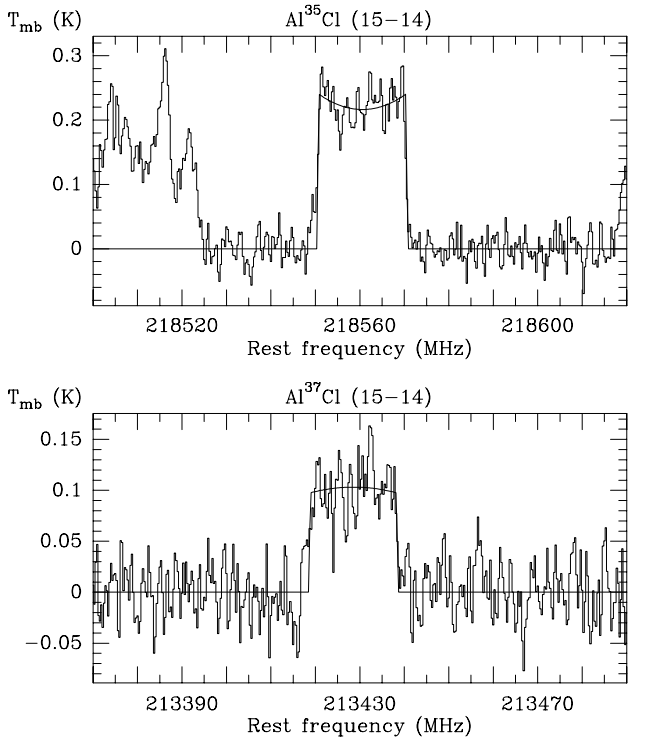

Fig. 2. The same as Fig. 1 for the AlCl (15-14) lines. The spectral resolutions are respectively 0.43 and 0.44 km s^{-1}.

spherical uniformly expanding envelopes, truncated parabolas, with positive or negative curvatures. The results and 1σ errorbars of the fits (frequencies, intensities at the line center, T^c_{mb}, integrated intensities, $\int T_{mb}\mathrm{d}v$, envelope expansion velocity, v_{exp}) are reported in Table 1, and the fitted profiles are plotted in Fig. 1 and Fig. 2.

The line profiles are quite rectangular, as expected for unresolved, optically thin, expanding envelope. As already mentioned by Cernicharo et al. (1987), the expansion velocities derived from the linewidths are smaller than the terminal velocity of 14.5 km s^{-1} derived for most molecular lines in IRC+10216, indicating that the lines arise from inner layers of the envelope, where the terminal velocity is not yet reached.

3. Results for the isotopic ratios

Assuming (i) that the lines are optically thin and (ii) that both isotopomers have the same excitation conditions (this is most likely, because their abundances are very similar), the derivation of the molecular abundance ratios from the integrated intensity ratios is straightforward: only a frequency correction (in ν^{-1}) has to be applied to take into account the frequency dependence of the line strengths (Kahane et al. 1988; 1992). The rms 1 σ errorbars on these ratios include two statistically independent uncertainties: a 10% calibration uncertainty and a "fit uncertainty". The results are reported in Table 2. We have also included in this table the molecular isotopic ratios obtained by Cernicharo et al. (1987) and two of the four ratios derived by Cernicharo et al. (2000) in the 2mm survey (two ratios based on tentatively detected lines have been ruled out). The five measurements appear to be compatible and no systematic difference between NaCl and AlCl (which would indicate an unlikely isotopic fractionation effect) can be seen. We conclude that these molecular abundance ratios reflect the elemental ^{35}Cl/^{37}Cl ratio. Using weightings inversely proportional to the individual errorbars, we derive an average ^{35}Cl/^{37}Cl ratio of 2.30 $\pm$ 0.24, significantly smaller than the solar value of 3.13. With the significantly reduced errorbars provided by the new data (the average of the previous data was 2.4 $\pm$ 0.4), we have been able to bring the first observational evidence that the AGB circumstellar envelope IRC+10216 presents deviations from the solar system isotopic composition that are not limited to the well known CNO isotopes. Furthermore, the accuracy of our ^{35}Cl/^{37}Cl isotopic ratio measurement allows now a meaningful comparison with theoretical predictions.

In Table 2 we have also reported the silicon and sulfur ratios derived from the 2mm survey (Cernicharo et al. 2000), which represent a significant improvement compared to previous estimates (Kahane et al. 1988) and, to our knowledge, the most accurate existing measurements of silicon and sulfur isotopic ratios in an evolved AGB star. We have further included the isotopic composition of C (Cernicharo et al. 2000), N (Kahane et al. 1988), O (Kahane et al. 1992), and Mg (Guélin et al. 1995).

Table 2. Observed isotopic ratios towards IRC+10216.

Ratio	Value	1 σ	Ref.[a]	Solar[b]
$Na^{35}Cl/Na^{37}Cl$ (7-6)	2.33	0.50	(1)	
$Al^{35}Cl/Al^{37}Cl$ (15-14)	2.15	0.33	(1)	
$Na^{35}Cl/Na^{37}Cl$ (8-7)	1.78	0.59	(2)	
$Al^{35}Cl/Al^{37}Cl$ (10-9)	3.17	0.79	(3)	
$Al^{35}Cl/Al^{37}Cl$ (11-10)	2.40	0.76	(3)	
$^{35}Cl/^{37}Cl$[c]	2.30	0.24	(1)	3.13
$^{12}C/^{13}C$	45	3	(3)	89
$^{14}N/^{15}N$	>4400		(4)	270
$^{16}O/^{17}O$	840	200	(5)	2610
$^{16}O/^{18}O$	1260	280	(5)	499
$^{24}Mg/^{25}Mg$	7.60	1.1	(6)	7.94
$^{24}Mg/^{26}Mg$	6.50	0.7	(6)	7.19
$^{29}Si/^{30}Si$	1.45	0.13	(3)	1.52
$^{28}Si/^{29}Si$[d]	>15.4		(3)	19.8
$^{34}S/^{33}S$	5.55	0.31	(3)	5.62
$^{32}S/^{34}S$	21.8	2.6	(3)	22.5

[a] the references are the following: (1) this paper; (2) Cernicharo et al. 1987; (3) Cernicharo et al. 2000; (4) Kahane et al. 1988; (5) Kahane et al. 1992; (6) Guélin et al. 1995

[b] from Anders & Grevesse 1989

[c] average value derived from the above ratios (see text)

[d] due to the non negligeable opacity of the ^{28}Si bearing lines, only a lower limit could be derived.

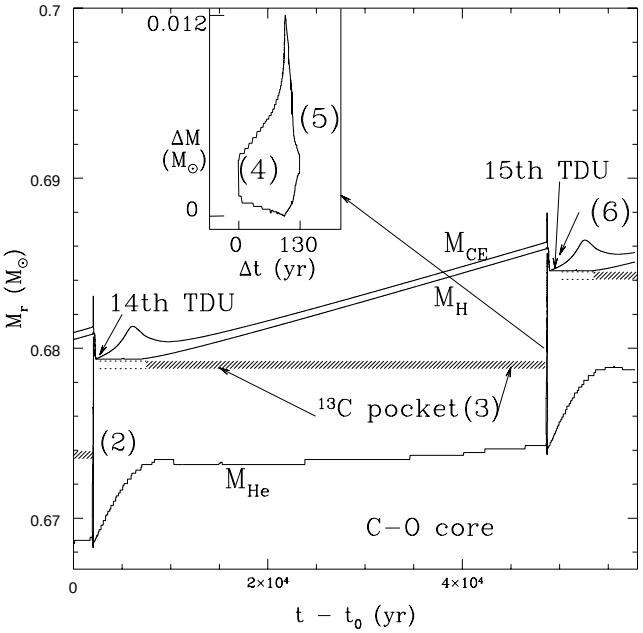

Fig. 3. Structure vs time of a AGB star model of 1.5 $M_\odot$ evolving trough the interpulse - pulse cycle illustrated in Table 3. The zero of the temporal scale in abscissa corresponds to $t_0 = 1.28\times10^8$ yr after the start of core He burning. M_r is the mass coordinate in $M_\odot$. The upper line (labelled $M_{\rm CE}$) represent the bottom of the convective envelope, the middle line (labelled $M_{\rm H}$) indicates the H/He discontinuity, and the bottom line (labelled $M_{\rm He}$) indicates the He/C-O core discontinuity. The zone comprised between the two last lines is the He intershell. The insert is an enlarged view of the $25^{\rm th}$ convective pulse, which precedes the $15^{\rm th}$ TDU episode. The shaded region corresponds to the layers of the ^{13}C pocket. For sake of clarity, this region was shifted somewhat downwards from the H/He discontinuity left by the TDU episode. There, a certain amount of protons are assumed to penetrate in the radiative He intershell (the proton pocket, corresponding to the area below TDU, not shaded). Immediately before H reignition protons are captured by the abundant ^{12}C , giving rise to the formation of a ^{13}C pocket. Before the next TP, all ^{13}C nuclei are consumed so that the ^{13}C pocket changes into an s pocket, before being ingested by the next growing convective instability. This structural scheme can be considered as representative of all AGB models with TDU, apart from numerical details. The bracketed numbers illustrate where and when the abundances reported in the corresponding column numbers of Table 3 were calculated.

4. Comparison with AGB model predictions

We used TP-AGB models obtained with the FRANEC evolutionary code for solar metallicity and initial masses 1.5, 3 and 5 $M_\odot$, adopting the Reimers' parameterization (Reimers 1975) for mass loss ($\eta = 0.7$, 1.5 and 10, respectively). In the 1.5 and 5 $M_\odot$ models, mass loss was actually accounted for in a post-process calculation, after computing the series of thermal pulses from a model with constant mass (Gallino et al. 1999). TDU was found to start at the 11th (1.5 $M_\odot$), 8th (3$M_\odot$) and 4th (5 $M_\odot$) thermal pulse, and the parameter λ was on average 0.24, 0.26 and 0.38 in the three cases. The model details are described elsewhere (Straniero et al. 1997; Gallino et al. 1998; Vaglio et al. 1998; Straniero et al. 2000).

In the most massive stellar model discussed here (the 5 $M_\odot$ star), the temperature at the base of the convective envelope during the interpulse never exceeds 50×10^6 K so that a negligible Hot Bottom Burning (HBB, i.e. burning at the inner edge of the convective envelope) occurs, without affecting the CNO nuclei. With FRANEC, efficient HBB is currently found in models of 6 and 7 $M_\odot$ and solar metallicity. The minimum mass for its activation decreases with decreasing metallicity (Lattanzio & Forestini 1999; Straniero et al. 2000).

As recalled in the introduction, in TP-AGB stars two neutron bursts are released in different conditions, by the ^{13}C and by the ^{22}Ne neutron source. The effectiveness of the ^{13}C neutron source requires the penetration of a limited amount of protons from the envelope into the He intershell zone at every TDU. This allows the formation of a tiny ^{13}C $pocket$ in the top layers of the He intershell at H-shell burning reignition. Subsequently, the ^{13}C nuclei are fully consumed by α-captures in radiative conditions already in the interpulse phase (Straniero et al. 1997). Though some successful models of the ^{13}C -pocket formation have been presented, the details are still a matter of debate (see for instance Herwig et al. 1997; Langer et al. 1999) and the amount of ^{13}C burnt per nucleosynthesis episode must be assumed as a free parameter of the model. However, this remarkable source of uncertainty does not affect much the resulting abundances of the nuclei discussed here, which mostly depend on the activation of the ^{22}Ne source, hence on the maximum temperature at the base of the TP convective zone, which in turn depends on the stellar mass. In order to illustrate this, in Fig. 3 we show the temporal evolution of the stellar struc-

Table 3. Enhancement factors with respect to initial abundances at the 25$^{\rm th}$ pulse of the 1.5 M$_\odot$ model, Z = 0.02.

N_i End 24th TP	He intershell	^{13}C pocket	He intershell Start 25th TP	He intershell End 25th TP	Envelope C/O = 1.3
^{24}Mg	1.048	1.662	1.072	1.048	1.002 (1.002)$^{(*)}$
^{25}Mg	56.60	29.12	22.61	62.04	1.110 (0.972)
^{26}Mg	2.974	6.008	2.103	3.196	1.050 (1.037)
^{28}Si	0.966	0.952	0.984	0.963	0.999 (0.999)
^{29}Si	1.514	0.974	1.176	1.556	1.013 (0.994)
^{30}Si	1.679	0.774	1.216	1.754	1.016 (0.994)
^{32}S	0.907	0.674	0.940	0.901	0.997 (0.999)
^{33}S	2.660	1.124	1.585	2.686	1.049 (1.006)
^{34}S	1.267	1.599	1.142	1.292	1.007 (1.002)
^{36}S	8.999	51.32	7.982	9.347	1.236 (1.205)
^{35}Cl	0.779	0.154	0.853	0.769	0.994 (0.996)
^{37}Cl	12.94	51.56	9.367	13.40	1.350 (1.216)
^{150}Sm	166.14	1270.08	164.41	172.11	5.866 (5.733)

* In brackets: test case with the ^{22}Ne source switched off.

ture during an interpulse - pulse cycle from our 1.5 M$_\odot$ model, while in Table 3 we present the enhancement factors with respect to solar of relevant isotopes across the same cycle. This corresponds to the interval between the 14th and the 15th TDU episode.

The phases shown include the end of the previous thermal pulse (24th, whose relevant abundances are listed in Column 2 of Table 3), the s processing through radiative burning inside the tiny ^{13}C pocket during the interpulse (Column 3) followed by dilution of the highly s-enriched pocket by a factor 20 in mass when the 25th convective TP spreads over the whole He intershell. Here the pocket is mixed with material composed at 50% of H-burning ashes and 50% of s-processed material (in the lower part of the He intershell) from the previous TPs. The composition after this dilution is shown in Column 4. Further s-processing occurs through partial ^{22}Ne burning in the TP. This occurs when the convective instability reaches its maximum extension, and lasts for about 6 yr. The final composition in the He intershell after the 25th TP is listed in Column 5.

From a comparison between the various columns one can understand which phases are dominant in the production of the various isotopes. Species lighter than Fe are controlled by ^{22}Ne burning, hence by the pulse temperature. In particular, for ^{26}Mg and ^{37}Cl the ^{22}Ne burning episode increases the previous abundance in the He intershell by a factor $\sim$ 1.5, and ^{25}Mg by a factor 2.7 (see Columns 4 and 5). The last column of the table gives the enhancement factor in the envelope after the 15th TDU episode, when C/O equals 1.3. Owing to dilution by TDU episodes with the original envelope, the surface enrichment with respect to solar at this stage is rather low, amounting to 11% and to 5%, respectively, in the case of ^{26}Mg and ^{26}Mg, and to 35% in the case of ^{37}Cl. Conversely, the most abundant isotopes ^{24}Mg and ^{35}Cl in the envelope are left about unchanged.

In the last column we also show (in brackets) the envelope enhancement factors resulting by the computation of a test case in which the ^{22}Ne(α,n)^{25}Mg reaction was switched off. By comparing the two numbers in Column 6 for each isotope one can see how much of the production factor in the envelope has to be ascribed to the ^{22}Ne source.

In the last row of Table 3 we have also included the heavy s-only isotope ^{150}Sm, in order to better state the difference between the heavy neutron-rich species and the lighter nuclei studied here. This last row shows that the abundance of ^{150}Sm is almost the same for the two cases of Column 6, since its production is dominated by the ^{13}C neutron source.

The observational results for Mg and Cl isotope ratios in the circumstellar envelope are compared in Fig. 4 with envelope predictions from the mentioned AGB models of two different initial mass and for different choices of the ^{13}C amount in the pocket (for silicon and sulfur, the measured and predicted ratios are compatible but will not be discussed here since the present observational errorbars are too large to provide any constrain on the models). Cases labelled ST correspond to the models defined as *standard* in Gallino et al. (1998) for stars up to 3 M$_\odot$, and in Vaglio et al. (1998) for intermediate mass AGB models. The other two are obtained by scaling the ^{13}C amount downward by a factor of three (d3), or upward by a factor of two (u2) (see Busso et al. 1999; Lugaro et al. 1999). In Fig. 4 each dot corresponds to a TDU episode; open symbols refer to the late TP-AGB phases where C/O $\geq$ 1.

The mass of the envelope is progressively eroded by stellar winds and in a minor way by the growing of the H-burning shell. The TDU mechanism ceases to operate when the envelope mass approaches 0.5 M$_\odot$. This corresponds to the last representative point shown in Fig. 4. There the photospheric ratios C/O and ^{12}C/^{13}C reach 1.4 and 63, respectively, for the 1.5 M$_\odot$ model, 1.1 and 103 for the 3 M$_\odot$ model, 1.3 and 122 for the 5 M$_\odot$ model. From then on the envelope composition does not change anymore, while the star will eventually encounter a phase of superwind (e.g., Iben & Renzini 1983) blowing off the remaining envelope. The cause of this phenomenon may be identified in a dynamical instability driven by radiation pressure

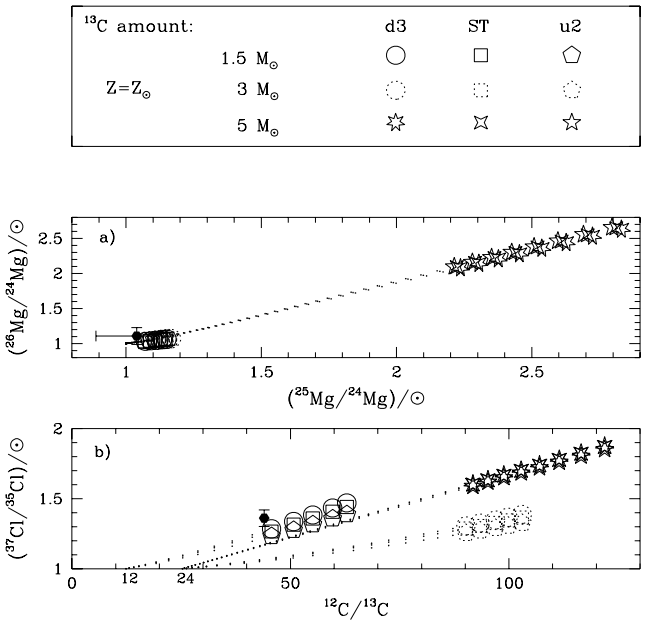

Fig. 4. a Computed isotopic ratios of ^{26}Mg/^{24}Mg vs ^{25}Mg/^{24}Mg during the TDU phases in the envelope of AGB stars of solar metallicity, initial masses 1.5, 3, and 5 M$_\odot$ and for different choices of the ^{13}C amount (d3, ST, u2, see Busso et al. 1999) as compared with measured isotopic ratios (full symbol). Large open symbols are for C-rich envelope, dots are for O-rich conditions. **b** The same as panel **a** for the ratio ^{37}Cl/^{35}Cl plotted versus ^{12}C/^{13}C.

right at the bottom of the envelope when the luminosity exceeds a critical value (Sweigart 1998; Straniero et al. 2000).

The results shown in Fig. 4 make clear that model predictions are almost independent of the amount of ^{13}C consumed in the pocket (see Lugaro et al. 1999 for a detailed discussion of the behaviour of Si isotopes). From Fig. 4 it appears that the 1.5 and 3 M$_\odot$ models are both compatible with the observed Cl and Mg isotopic ratios, whereas the 5 M$_\odot$ model predicts too high values for the ^{37}Cl/^{35}Cl and ^{25,26}Mg/^{24}Mg ratios with respect to the observations.

Let us discuss the above result in the more general context of AGB modelling. The final Cl and Mg abundances in the envelope might in principle depend of the choices for TDU and mass loss as well as on the efficiency of the ^{22}Ne neutron source during the TPs. As it is well known the lack of a reliable theory for stellar convection and the difficulty of evaluating a suitable mass loss rate may substantially affect our comprehension of AGB evolution. The models here adopted have been computed by using the Schwarzschild criterion for convection, without allowing for any extramixing. This likely provides a minimal efficiency for TDU. We have also used the Reimers' formula to account for the mass loss rate. Other stellar evolutionary models make use of various diffusive or overshoot prescriptions for TDU (e.g., Frost & Lattanzio 1996; Herwig et al. 1997), and of different mass loss criteria.

We can have hints on the effects that a more efficient TDU in the first TPs may have on the predicted isotopic ratios by considering how these last vary from pulse to pulse. For the 1.5 M$_\odot$ model the abundance by mass of ^{37}Cl in the He intershell varies from the 15.th TP (5.th with TDU) to the 25.th TP by a factor 1.5. This increase is related to the slight progressive increase of the peak temperature at the bottom of the TPs, from 2.78 $\times$ 10^8 K at the 15.th TP to 2.99 $\times$ 10^8 K at the 25.th TP. Other factors are involved, such as the decrease with pulse number of the mass of the He intershell and of the overlap factor among adjacent pulses (e.g., Gallino et al. 1998). All these structural chacteristics are quite general in low mass AGB stars, being governed by the relatively low value of $M_{\rm H}$ at the first TP with TDU (e.g., Gallino et al. 1998). In models with a more efficient TDU since the first TPs, and a lower number of pulses on the AGB so that about the same final carbon enrichment in the envelope would result, the ^{37}Cl abundance in the envelope might achieve a slightly lower surface enrichment than we do. However, because of dilution with the envelope the effect is not large and our general conclusions would not change. In the case of the 5 M$_\odot$ model, the value of $M_{\rm H}$ at the first TDU is already 0.88 M$_\odot$, and the various structural and physical characteristics in the He intershell, among which the temperature history in the TPs, remain almost the same from pulse to pulse (Straniero et al. 2000). Thus the abundances of Cl isotopes in the He intershell reach asymptotic values very quickly, so that any choice for TDU and mass loss would lead to a too high ^{37}Cl/^{35}Cl ratio at the stellar surface to be compatible with observations. Similar considerations hold for the Mg isotopes.

We therefore argue that, as for the constraints derived from Cl and Mg isotopes, a higher mass estimate for CW Leo is possible only from models where the temperature in the pulses, the temporal evolution of the mass of the He intershell and overlap between adjacent TPs, or the rate of the ^{22}Ne(α,n)^{25}Mg reaction (i. e. the fundamental structural parameters in the TP-AGB phase), are substantially different than in our model. Whether these differences are possible is something that deserves scrutiny in another context. In any case, the precision of the new Cl measurement allows us to reduce the ambiguity on the initial stellar mass, showing that this last has to be low enough to keep at low efficiency the ^{22}Ne neutron source. With the models presently adopted this actually requires a mass below 3 M$_\odot$.

A further comment concerns the luminosity. Our 1.5 M$_\odot$ model reaches a maximum luminosity at the tip of the TP-AGB phase of 1.15 $\times$ 10^4 L$_\odot$, which fits in the range deduced by observations. On the contrary, our 5 M$_\odot$ is too luminous (4.15 $\times$ 10^4 L$_\odot$). This is another argument in favour of a low initial mass.

5. Constraints from CNO isotopes

5.1. The ^{12}C/^{13}C *ratio*

In Fig. 4 we plotted the envelope Cl isotopic ratio versus the ^{12}C/^{13}C ratio, with two different initial ratios at the beginning of the TP-AGB phase: (^{12}C/^{13}C)$_{ini}$ = 12, or 24, as representative of low-mass AGB stars ($M \leq 2$ M$_\odot$) or of higher mass stars, respectively. This important point needs to be elucidated.

IRC+10216 has a ^{12}C /^{13}C ratio of 45 $\pm$ 3 (see Table 2). This value, which is typical of C (N-type) stars with measured

C/O $\approx$ 1 (e.g., de Laverny & Gustafsson 1998; Lambert et al. 1986; Jorissen et al. 1992) may appear a bit small in the case of IRC+10216, if we accept for it the value C/O = 1.4 inferred from circumstellar modelling (Winters et al. 1994). The estimated C/O ratio is reasonable in the lights of the advanced spectral type of CW Leo (C9.5, see Olofsson et al. 1982) but cannot be trusted at the same level of confidence as the other (observed) ratios discussed here. Therefore, independently of the precise C/O value, we shall simply try to explain how a C-rich atmosphere with the observed ^{12}C /^{13}C ratio can be formed.

It is known that in the red giant phase the ^{12}C /^{13}C ratio is modified by the first dredge up, where a photospheric value $\sim 20 - 25$ is predicted by canonical models. This implies that later, on the TP-AGB, mixing of pure ^{12}C by TDU would increase this isotopic ratio to values around 100. However, in red giant stars of low mass ^{12}C /^{13}C values lower than the canonical one have been measured spectroscopically (Gilroy 1989). For stars on the red giant branch and initial masses below ~ 2 M$_\odot$, an appropriate value for the ^{12}C /^{13}C ratio appears to be between 10 and 15. This indicates that some kind of extramixing, or "cool bottom processing" (CBP) phenomena are at work (Charbonnel 1994, 1995; Wasserburg et al. 1995; Charbonnel et al. 1998), possibly driven by rotational shear (Sweigart & Mengel 1979).

From Fig. 4b it results that CBP, simulated by adopting a ^{12}C /^{13}C value of 12 on the red giant branch, chosen as appropriate for a low mass model, is indeed required to explain the observed carbon isotope ratio in the circumstellar envelope of CW Leo. We notice that in the case of the 1.5 M$_\odot$ model we predict for this ratio the value of 45 when C/O equals unity (i.e. slightly less than the C/O ratio estimated for CW Leo), at a somewhat earlier phase than the AGB tip. However, in view of the above discussion on C/O this cannot be considered as critical. It would be sufficient in our models to change the η parameter of mass loss, increasing it slightly, to obtain C/O $= 1$ and ^{12}C /^{13}C $= 45$ at the very end of the sequence. Another possibility is to choose a slightly higher progenitor mass, resulting in a somewhat larger dilution of He-intershell material with the envelope. In the absence of a precise measurement for the C/O ratio in CW Leo, all we can say is that our 1.5 M$_\odot$ AGB model can provide a C-rich envelope with the observed ^{12}C /^{13}C ratio. Conversely, in AGB stars of $M > 2$ M$_\odot$, this is not possible, as the observational evidence excludes the operation of CBP. In stars with $M > 2$ M$_\odot$ the ^{12}C /^{13}C ratio reaches about 100 already at C/O $= 1$.

Thanks to CBP, the same low mass star holds to explain the high value of the ^{14}N/^{15}N ratio (Boothroyd et al. 1995), for which only a lower limit exists. In principle, the predicted ^{12}C /^{13}C ratio in the AGB phase might be kept low also for higher stellar masses, but only if a moderate HBB occurs, consuming some of the ^{12}C in the envelope (Guélin et al. 1995; Weigelt et al. 1998).

5.2. The ^{16}O/^{17}O and ^{16}O/^{18}O ratios

Another crucial constraint comes from the oxygen isotopes, and this is a further decisive argument in favour of a low initial mass. Indeed, as shown by Boothroyd et al. (1995) and Lattanzio & Boothroyd (1997), the low value of ^{16}O/^{17}O, and the high value of ^{16}O/^{18}O measured in IRC+10216 (see Table 2) cannot be explained by HBB, even of moderate entity. When represented in a 3-isotope plot displaying the ^{18}O/^{16}O ratio versus the ^{17}O/^{16}O one, the data (see Fig. 2 of Wasserburg et al. 1995) falls in a region that cannot be reached by model curves from HBB calculations. The same authors show instead as those isotopic ratios, which are not accounted for by the canonical first dredge up, are a natural result of CBP. This fact again necessarily implies a low initial mass.

As a final comment, it can be noticed that our conclusion about a low initial mass for CW Leo places it in the already known family of dust-enshrouded low-mass carbon stars. This was indirectly recognized through high precision isotopic measurements in presolar SiC grains recovered from meteorites (Zinner 1997; Hoppe & Ott 1997), while comparisons with nucleosynthesis models similar to the one performed here demonstrated that indeed these grains condensed in the circumstellar envelopes of low-mass carbon stars (Gallino et al. 1997).

6. Conclusions

New observations of four transitions, belonging to two chlorine bearing molecules, have allowed to derive an accurate and reliable measurement of the ^{35}Cl/^{37}Cl ratio towards IRC+10216, the circumstellar envelope of the carbon-rich AGB star CW Leo. It represents the first observational evidence for a significant deviation from solar of an isotopic ratio of elements heavier than the CNO in this circumstellar envelope. The high accuracy of the new data presented here for Cl, combined with the carbon and magnesium isotopic ratios previously measured in IRC+10216, allow nucleosynthesis models to constrain the initial stellar mass better than previously possible (Guélin et al. 1995; Forestini & Charbonnel 1997). The inferred mass is low, $M \leq 2$ M$_\odot$, as often assumed in IRC+10216 envelope modelling. Our results are obtained with the Reimers (1975) choice for the mass loss rate and with the TDU efficiency provided by the Schwarzschild criterion inside the FRANEC evolutionary code. We have argued, from the dependence of Cl isotope abundances on the pulse number, and from independent constraints provided by carbon, magnesium and oxygen isotopes, that our results for the stellar mass remain valid independently of several details (mass loss prescriptions, TDU) of the specific stellar code adopted. A dedicated check from s-process calculations in different evolutionary codes would be clearly useful.

Acknowledgements. We are indebted to an anonymous referee for useful suggestions. It is a pleasure to thank Dr. Uli Ott for his careful and useful check of the manuscript. This work was partly supported by the MURST Italian grant Cofin98. ML gratefully acknowledges the support of a OPRS grant.

References

Anders E., Grevesse N., 1989, Geochim. Cosmochim. Acta 53, 197
Boothroyd A.I., Sackmann I.-J., Wasserburg G.J., 1995, ApJ 442, L21
Busso M., Lambert D.L., Beglio L., et al., 1995, ApJ 446, 775

Busso M., Gallino R., Wasserburg G.J., 1999, ARA&A 37, 239
Cernicharo J., Guélin M., Kahane C., 1987, A&A 183, L10
Cernicharo J., Guélin M., Kahane C., 2000, A&AS in press
Charbonnel C., 1994, A&A 283, 811
Charbonnel C., 1995, ApJ 453, L41
Charbonnel C., Brown J.A., Wallerstein G., 1998, A&A 332, 204
de Laverny P., Gustafsson B., 1998, A&A 332, 661
Forestini M., Charbonnel C., 1997, A&AS 123, 241
Frost C.A., Lattanzio J.C., 1996, ApJ 473, 383
Gallino R., Busso M., Lugaro M., 1997, In: Bernatowicz T.J., Zinner E. (eds.) Astrophysical Implication of the Laboratory Study of Presolar Materials. AIP Conf. Proc. 402, AIP, Woodbury, p. 115
Gallino R., Arlandini C., Busso M., et al., 1998, ApJ 497, 388
Gallino R., Busso M., Lugaro M., Travaglio C., Straniero O., 1999, In: Noels A., et al. (eds.) The Galactic Halo from Globular Clusters to Field Stars. 35 Liège Int. Astroph. Coll., Institut d'Astrophysique, Liège, in press
Gilroy K.K., 1989, ApJ 347, 835
Groenewegen M.A.T., van der Veen W.E.C.J., Matthews H.E., 1998, A&A 338, 491
Guélin M., Forestini M., Valiron P., Ziurys L.M., Anderson M.A., 1995, A&A 297, 183
Herwig F., Blöcker T., Schönberner D., El Eid M., 1997, A&A 324, L81
Hoppe P., Ott U., 1997, In: Bernatowicz T.J., Zinner E. (eds.) Astrophysical Implication of the Laboratory Study of Presolar Materials. AIP Conf. Proc. 402, AIP, Woodbury, p. 27
Iben I. Jr., 1975, ApJ 196, 525
Iben I. Jr., Renzini A., 1983, ARA&A 21, 271
Iben I. Jr., Truran J.W., 1978, ApJ 220, 980
Jorissen A., Smith V.V., Lambert D.L., 1992, A&A 261, 164
Kahane C., Gomez-Gonzales J., Cernicharo J., Guélin M., 1988, A&A 190, 167
Kahane C., Cernicharo J., Gomez-Gonzales J., Guélin M., 1992, A&A 256, 235
Lambert D.L., Gustafsson B., Eriksson K.H., Hinkle K.H., 1986, ApJS 62, 373
Langer N., Heger A., Wellstein S., Herwig F., 1999, A&A 346, L37
Lattanzio J.C., Boothroyd A., 1997, In: Bernatowicz T.J., Zinner E. (eds.) Astrophysical Implication of the Laboratory Study of Presolar Materials. AIP Conf. Proc. 402, AIP, Woodbury, p. 85
Lattanzio J.C., Forestini, M., 1999, In: Le Bertre T., Lèbre A., Waelkens C. (eds.) Asymptotic Giant Branch Stars. IAU Symp. 411, ASP, Provo, p. 31
Le Bertre T., 1997, A&A 324, 1059
Lugaro M., Zinner E., Gallino R., Amari S., 1999, ApJ 527, 369
Merrill P.W., 1952, Sci 115, 484
Olofsson H., Johansson L.E.B., Hjalmarsson A., Rieu N.Q., 1982, A&A 107, 128
Reimers D., 1975, Mém. Soc. R. Sci. Liège Ser. 6, 8, 369
Skinner C.J., Meixner M., Bobrowsky M., 1998, MNRAS 300, L29
Straniero O., Chieffi A., Limongi M., et al., 1997, ApJ 478, 332
Straniero O., Limongi M., Chieffi, et al., 2000, In: D'Antona F., Gallino R. (eds.) The Changes in Abundances AGB Stars. Mem. Soc. Astron. Ital., in press
Sweigart A.V., Mengel J.G., 1979, ApJ 229, 624
Sweigart A.V., 1998, IAU 191, 553
Truran J.W., Iben I. Jr., 1977, ApJ 216, 797
Vaglio P., Gallino R., Busso M., et al., 1998, In: Harissopulos S., Prantzos N. (eds.) Nuclei in the Cosmos V, Editions Frontières, Paris p. 223
Wasserburg G.J., Boothroyd A., Sackmann J., 1995, ApJ 447, L37
Weigelt G., Balega Y., Blöcker T., et al., 1998, A&A 333, L51
Winters J.M., Dominik C., Sedlmayr E., 1994, A&A 288, 255
Zinner E., 1997, AREPS 26, 147